Coastal Engineering 57 (2010) 656–667

Contents lists available at ScienceDirect

Coastal Engineering

journal homepage: www.elsevier.com/locate/coastaleng

Analytical approximate wave form for asymmetric waves

Tiago Abreu [a,*], Paulo A. Silva [b], Francisco Sancho [c], André Temperville [d]

[a] Department of Civil Engineering, Polytechnic Institute of Viseu, ESTV Campus de Repeses, Viseu, 3504-510, Portugal
[b] CESAM & Department of Physics, University of Aveiro, 3810-193 Aveiro, Portugal
[c] LNEC-DHA, National Civil Engineering Laboratory, Av. do Brasil, 101, Lisboa, 1700-066, Portugal
[d] Laboratoire des Ecoulements Géophysiques et Industriels, B.P.53, 38041 Grenoble Cedex 9, France

ARTICLE INFO

Article history:
Received 22 August 2009
Received in revised form 5 February 2010
Accepted 12 February 2010
Available online 19 March 2010

Keywords:
Wave skewness
Wave asymmetry
Acceleration skewness
Orbital velocity
Cnoidal wave
Sawtooth profile

ABSTRACT

A simple analytical formulation that reproduces a skewed, nonlinear near-bed wave orbital velocity is presented. It contains four free parameters, where two are solely related to the velocity and acceleration skewnesses. The equation is compared with other models and is validated against field and laboratory experiments. The results reveal that it can simulate a wide range of nonlinear wave shapes, reproducing satisfactorily the measured nonlinear wave particle velocity. Also, the new expression overcomes some limitations of the other models. The new formulation is therefore capable of being used in many engineering applications that require the use of representative wave forms.

1. Introduction

Wave motion in water is one of the most fascinating physical phenomena in nature. The wave dynamics in shallow water has long been pursued by mathematicians, physicists and engineering scientists, leading to the development of different nonlinear mathematical theories and equations (e.g., Boussinesq and Korteweg–de Vries equations).

Stokes (1847) was one of the first to note the nonlinearities prior to wave breaking. He observed that, as waves approach the coast and propagate into shallower water, the waves present shorter and higher crests and longer and shallower troughs. This asymmetric shape gives rise to skewed wave orbital velocities that can be expressed in terms of a velocity skewness coefficient, R, defined as:

$$R = \frac{u_{max}}{u_{max} - u_{min}} \tag{1}$$

where u is the horizontal flow velocity and u_{max} and u_{min} are the u values at the crest and trough, respectively. For symmetric waves R equals 0.5, whereas when the magnitude of velocity at the crest is larger than that at the trough, $R>0.5$. The case of $R<0.5$ occurs when the absolute value of the velocity at the trough is larger than that at the crest, which is less common in nearshore propagating waves.

In addition, several measurements show that breaking and surf zone waves present a sawtooth-shaped surface profile (e.g., Svendsen et al., 1978; Elgar and Guza, 1985), with large values of velocity skewness and differences between crest-to-trough and trough-to-crest half periods (e.g., Torres-Freyermuth et al., 2007). This last kind of vertical asymmetry can be formulated in terms of an acceleration skewness coefficient, β, whose definition is analogous to Eq. (1):

$$\beta = \frac{a_{max}}{a_{max} - a_{min}} \tag{2}$$

where a_{max} and a_{min} have the same meaning as in Eq. (1), but for the fluid horizontal acceleration, a. Acceleration-wise symmetric waves present $\beta = 0.5$, which corresponds to waves whose maximum and minimum acceleration magnitudes are equal.

Other parameters describing the wave acceleration skewness have been proposed in the literature, for example, the "velocity-leaning index" β_{cw} (Watanabe and Sato, 2004), defined as:

$$\beta_{cw} = 1 - \frac{2T_{pc}}{T} \tag{3}$$

and the "wave skewness parameter" α (Suntoyo, et al., 2008), closely related to β_{cw}:

$$\alpha = 2T_{pc}/T = 1 - \beta_{cw} \tag{4}$$

* Corresponding author. Fax: +351 232424651.
E-mail addresses: tabreu@estv.ipv.pt (T. Abreu), psilva@ua.pt (P.A. Silva), fsancho@lnec.pt (F. Sancho), andre.temperville@hmg.inpg.fr (A. Temperville).

0378-3839/$ – see front matter © 2010 Elsevier B.V. All rights reserved.
doi:10.1016/j.coastaleng.2010.02.005

In the above, T_{pc} is the time interval measured from the zero up-cross point to wave crest in the time variation of free-stream velocity, and T is the wave period.

Based on a large number of field measurements at the nearshore zone, Elfrink et al. (2006) have determined that the range of the nonlinear parameters were within $0.51 \le R \le 0.66$ and $0.22 \le \alpha \le 0.54$. These findings confirm, thus, the importance of wave asymmetries in the nearshore.

Improved knowledge and description of the hydrodynamics and sediment transport in the nearshore zone is crucial to beach evolution predictions. Van der A et al. (2008) analysed the effects of acceleration skewness on a rough fixed-bed oscillatory boundary layer flow and found that it leads to asymmetric bed shear stresses. The asymmetries of the wave shape and the induced near-bed flow are related to sediment transport as shown by the experimental works of Ribberink and Al-Salem (1994), Watanabe and Sato (2004) and Silva et al. (2008). Also, the knowledge of such wave motion in water is required for several practical sediment transport formulae (e.g., Bailard, 1981; Hoefel and Elgar, 2003; Soulsby and Damgaard, 2005; Silva et al., 2006; Nielsen, 2006). Moreover, Hsu and Hanes (2004) concluded that the sediment transport process may strongly depend on the wave shape and cannot be fully described solely by the magnitude of free-stream velocity. Finally, the importance of wave asymmetries in morphodynamic features, like sandbar migrations, has also been recognized (Elgar et al., 2001).

All these nonlinear wave effects can be obtained from detailed wave models (e.g., Boussinesq models and RANS models) that describe the transformation of waves as they approach the shore. However, these models can be computationally demanding and for practical engineering purposes a representation of the wave based on simple analytic theories (linear and nonlinear theories) is often considered.

The main purpose of the present work is to propose a new simple analytical expression that can replicate both velocity and acceleration asymmetries similar to those found in shallow water waves. The new expression is compared with previous ones developed by Isobe and Horikawa (1982), Drake and Calantoni (2001) and Elfrink et al. (2006), which turn out to be particular cases of the present more general formula. The simplicity inherent in the new formulation allows the generation and reproduction in wave flumes, or water tunnels, of shallow water waves with several nonlinear shapes, as found in nature. The formula contains 4 free parameters, 2 related to the orbital velocity amplitude and wave period and two related to the velocity and acceleration asymmetries, R and α. In the literature it is possible to find several publications that provide (R, α) as a function of commonly used parameters such as wave height, wave period, local water depth and local bottom slope (e.g., Dibajnia et al., 2001; Tajima and Madsen, 2002; Tajima, 2004; Elfrink et al., 2006) therefore enabling the practical application of this formulation. Acceleration-skewed waves has already been performed in the Large Oscillating Water Tunnel (LOWT) of WL|Delft Hydraulics by Silva et al. (2008) using this new expression. The proposed wave form can also be used for the wave-generating boundary conditions in detailed wave-propagation models (e.g., Ruessink et al., 2009), and in sediment transport parameterisations.

The following section starts with a description and analysis of the new formulation. It is followed in the third section by an examination of the relations between the macro waveform parameters presented earlier (R, α, and β), and the direct input parameters of the new formula. In the fourth section, the new expression is tested against different theoretical wave formulations found in the literature. Next, the new wave form is applied to reproduce the time series of measured near-bed velocities, of both a field and a laboratory experiment. Finally, conclusions are drawn.

2. Analytical description of nonlinear waves

Because natural waves in the nearshore often present both velocity and acceleration skewnesses, a simple analytical formulation for the near-bed orbital velocity that accounts for both asymmetries is developed. The expression intends to reproduce the horizontal velocity above the wave boundary layer which is generally only a small fraction of the water depth, of the order of a few ten centimetres in thickness (Nielsen, 1992).

The new formula is based on the work of Drake and Calantoni (2001), who considered a near-bed orbital velocity representative of a wide range of shoaling and broken waves proportional to:

$$u(t) \propto \sum_{k=0}^{4} \frac{1}{2^k} \sin\left[(k+1)\omega t + k\phi\right] \tag{5}$$

where k represents an integer value, $\omega = 2\pi/T$ is the angular frequency and ϕ is a waveform parameter ($-\pi/2 \le \phi \le \pi/2$) related to the biphase (e.g., Elgar and Guza, 1985; Leykin et al., 1995). In their work, Drake and Calantoni (2001) presented three particular cases of ϕ: (i) $\phi = 0$, resulting in an accelerated skewed wave (sawtooth wave profile); (ii) $\phi = -\pi/2$, approaching the case of a velocity-skewed wave (with a velocity shape similar to that of a 1st-order cnoidal wave); and (iii) $\phi = -\pi/4$, corresponding to a wave with both velocity and acceleration skewnesses.

One can generalize Eq. (5) and admit that the velocity is given by:

$$u(t) = U_w \sum_{k=0}^{\infty} \frac{1}{n^k} \sin\left[(k+1)\omega t + k\phi\right] \tag{6}$$

where U_w represents the amplitude of the orbital velocity, $U_w = (u_{max} - u_{min})/2$ and n is a parameter that allows changing the wave acceleration and velocity skewness. In the formulation of Drake and Calantoni (2001) $n = 2$, which corresponds to fixed values of R and β for each ϕ, as described in Section 4.2.

As given in Appendix A, this summation can be exactly computed within the framework of analytical functions of complex variables, yielding:

$$u(t) = U_w f \frac{\left[\sin(\omega t) + \dfrac{r\sin\phi}{1+\sqrt{1-r^2}}\right]}{\left[1 - r\cos(\omega t + \phi)\right]} \tag{7}$$

The parameter r is an index of skewness or nonlinearity ($-1 < r < 1$) and is related with n by $r = 2n/(1+n^2)$. The variable f in Eq. (7) is a dimensionless factor, function of r $\left(f = \sqrt{1-r^2}\right)$, allowing the velocity amplitude to be equal to U_w. There is no simple relation between r and the skewness parameters proposed, R and β. As described further in this section, an analytical approximate formulation can be found, relating both parameters for some particular cases of ϕ. Also, a procedure to determine r and ϕ from the knowledge of R and α is devised in the third section.

The corresponding acceleration time series of Eq. (7) is given by

$$a(t) = U_w \omega f \frac{\cos(\omega t) - r\cos\phi - \dfrac{r^2}{1+\sqrt{1-r^2}}\sin\phi\sin(\omega t + \phi)}{\left[1 - r\cos(\omega t + \phi)\right]^2} \tag{8}$$

Figs. 1 and 2 show examples of the shape of time varying orbital velocities and accelerations calculated from Eqs. (7) and (8), respectively, for a number of intervals in the r and ϕ domain ($r = [0, 0.25, 0.5, 0.75]$, $\phi = [0, -\pi/4, -\pi/2]$). Clearly, it is possible to deduce that, independently of ϕ values, Eq. (7) matches the sinusoidal wave for $r = 0$. However, when r increases, the nonlinear behaviour is evidenced. The particular cases of $\phi = -\pi/2$ and $\phi = 0$ correspond to two wave formulations, respectively, the skewed wave forcing, with

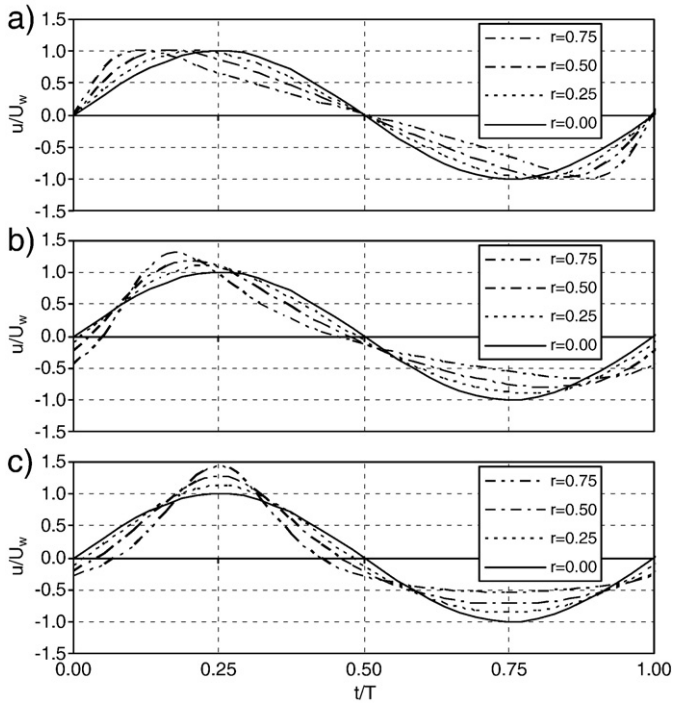

Fig. 1. Time varying orbital velocity for different values of index of skewness r and ϕ: a) $\phi=0$; a) $\phi=-\pi/4$; c) $\phi=-\pi/2$.

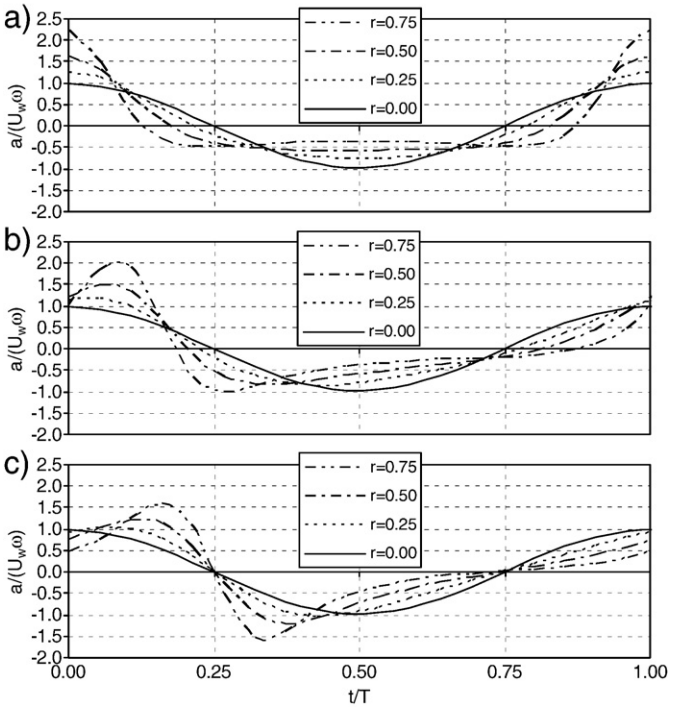

Fig. 2. Time varying orbital acceleration for different values of index of skewness r and ϕ: a) $\phi=0$; a) $\phi=-\pi/4$; c) $\phi=-\pi/2$.

the shape of a 1st-order cnoidal wave, and the sawtooth profile described by Drake and Calantoni (2001).

For $\phi=-\pi/2$, Eq. (7) reduces to the following equation:

$$u(t)=U_w f\frac{\left[\sin(\omega t)-\frac{r}{1+\sqrt{1-r^2}}\right]}{[1-r\sin(\omega t)]} \tag{9}$$

with the corresponding acceleration time series

$$a(t)=U_w\omega f\frac{\cos(\omega t)-\frac{r^2}{1+\sqrt{1-r^2}}\cos(\omega t)}{[1-r\sin(\omega t)]^2} \tag{10}$$

Eq. (9) gives a velocity time series with a shape similar to that of a 1st-order cnoidal wave (Fig. 1c) in a way that only accounts for the velocity skewness. Given the definition (1), it is possible from Eq. (9) to obtain a relation between R and r, yielding:

$$R=\frac{(1+r)\left(1-r+\sqrt{1-r^2}\right)}{2\left(1-r^2+\sqrt{1-r^2}\right)} \tag{11}$$

A similar calculation of β through definition (2) and Eq. (10) results in $\beta=0.5$ for this particular case ($\phi=-\pi/2$).

Elfrink et al. (2006) further point out that the shape of the velocity distribution between the wave crest and the zero down-crossing is usually concave and not convex. The present function clearly shows this behaviour for the $r>0.25$ (Fig. 1c).

For $\phi=0$, Eq. (7) reduces to the following equation:

$$u(t)=\frac{U_w\sqrt{1-r^2}\sin(\omega t)}{[1-r\cos(\omega t)]} \tag{12}$$

For this wave, the orbital velocity is symmetric with respect to the horizontal axis (velocity skewness is zero: $R=0.5$) but is asymmetric with respect to the vertical axis within each half cycle, which gives rise to skewed accelerations ($\beta\neq0.5$). Following Drake and Calantoni (2001), this wave is characteristic of surf zone bores.

The previous wave form (Eq. (12)) was already proposed by Silva et al. (2007), apart the coefficient $f=\sqrt{1-r^2}$, assuming that the sawtooth wave acceleration time series is similar to the velocity profile of a 1st-order cnoidal wave. The acceleration corresponding to Eq. (12) is given by:

$$a(t)=\frac{U_w\omega\sqrt{1-r^2}[\cos(\omega t)-r]}{[1-r\cos(\omega t)]^2} \tag{13}$$

From Eq. (13) it is possible to obtain a relation between β and r, yielding:

$$\beta=\begin{cases}(1+r)/2 & ,r\leq0.5\\ 4r(1+r)/(1+2r)^2 & ,r>0.5\end{cases} \tag{14}$$

For completeness, we compare in Fig. 3 the results from the above formulae (Eqs. (9) and (13)) with those from 1st-order cnoidal wave theory (from Svendsen, 2006, pp. 396–406). In detail, the left panel shows the results from Eq. (9), for various r values ($0\leq r\leq0.8$), against the cnoidal wave solution for various Ursell numbers ($0.05\leq U_r\leq120$). No match in the nonlinear parameters was pursued between these solutions, although according to Eq. (11) the results from Eq. (9) correspond to the range $0.5\leq R\leq0.75$, and those from the 1st order cnoidal wave theory correspond to $0.55\leq R\leq0.75$. For the lower values of r, the present solution is a good approximation of a cnoidal wave shape, whereas for $r>0.6$ it exhibits a form deviating significantly from the cnoidal wave.

In the right panel of Fig. 3 one observes a comparison between the non-dimensional acceleration time series as given by Eq. (13), for the same range of r values, and the exact cnoidal wave solution. In general, this solution, which is the particular case of Eq. (8) for $\phi=0$, compares favourably with the exact solution for low values of r. For values of $r>0.6$ a second local maximum at $t=0.5\,T$ is apparent in the results from the approximated function, leading to a convex-curve shape at the wave trough, instead of the expected concave shape as

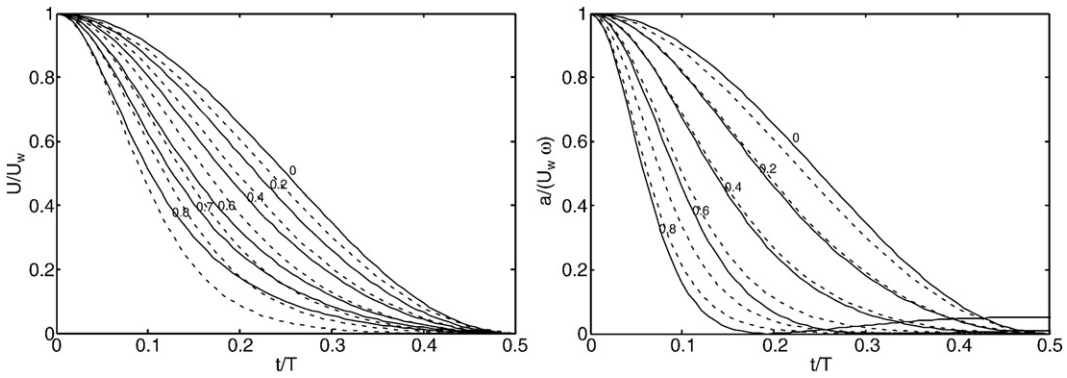

Fig. 3. Half-period time variation of present approximate functions (—), for $0 \le r \le 0.8$ (see labels in figure), and exact cnoidal wave (---) for various Ursell numbers ($0.05 \le U_r \le 120$). Left: velocity given by Eq. (9); Right: acceleration given by Eq. (13).

shown in Fig. 2a for $r = 0.75$. It may be therefore recommended to restrict the use of expression (7) to values $-0.6 < r < 0.6$, keeping in mind that negative values of r cause a sharp trough and a flat crest.

For values of ϕ between $\phi = 0$ and $\phi = -\pi/2$, expression (7) yields a wave form with both velocity and acceleration skewnesses ($R \neq 0.5$ and $\beta \neq 0.5$), (see Figs. 1b and 2b).

Figs. 1 and 2 show that the velocity skewness increases while the acceleration skewness decreases for increasing values of $|\phi|$. Thus, the waveform parameter ϕ expresses the relative importance of both skewnesses. Negative values of r or positive values of ϕ lead to temporal shifts and reversals to the asymmetric wave shape as shown and clarified in Fig. 4. In the upper panel, the influence of r is presented. The negative value of r causes a reflected image in relation to the horizontal axis and a phase shift of $t/T = 0.5$. In the lower panel, the influence of ϕ is presented and it is perceptible that a positive value of ϕ reproduces a wave profile that is reflected both horizontally and vertically.

Finally, the new function fulfils the requirement of zero mean velocity and was already used in forcing the flow velocity in the sand transport experiments conducted in the Large Oscillating Water Tunnel (LOWT) of WL|Delft Hydraulics (Silva et al., 2008), with or without a net current added.

3. Parameterisations of input parameters

The new formulation presented above allows us to represent several nonlinear wave profiles through the introduction of two parameters: ϕ and r. For the particular cases $\phi = 0$ and $\phi = -\pi/2$ it has been shown that one can relate analytically the nonlinear index r with the usual macroscopic wave skewness parameters R and β (see Eqs. (11) and (14)). A similar analysis could be performed for other intermediate values of ϕ, but the results would become forbiddingly unmanageable, justifying the use of simple parameterisations. Therefore, this section presents general parameterisations of R and β as functions of r, for (certain) values of ϕ within that range. The analysis is also extended to the commonly used "wave skewness parameter", α (Eq. (4)). The expressions concern the principal range of application of those parameters, i.e., for $R \ge 0.5$, $\beta \ge 0.5$ and $\alpha \le 0.5$.

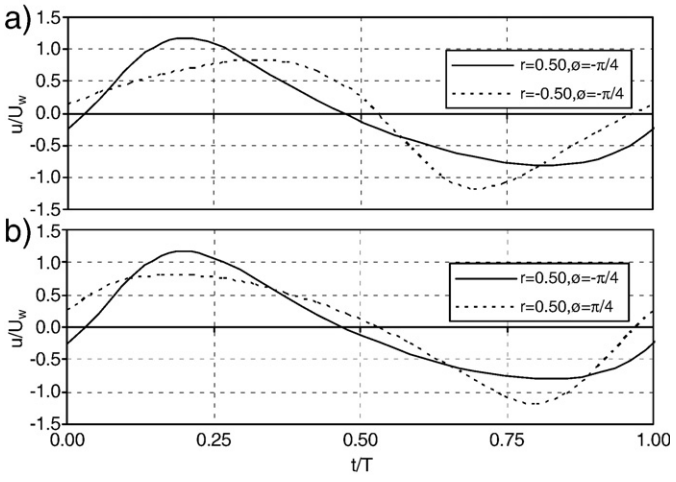

Fig. 4. Time varying orbital velocities for $\phi = -\pi/4$ and $r = 0.5$ showing the influence of r negative values or ϕ positive values.

Regarding Eq. (7), the relations between r and R, β and α are constructed by varying ϕ, as presented in Fig. 5.

Focusing on r *versus* R, for $\phi = 0$ the outcome is $R = 0.5$ for all values of r (velocity under the crest equal to the velocity under the trough). For the other values of ϕ it is possible to see that the relation between the two parameters is almost linear for $r \le 0.5$ but increasingly non-linear for $r > 0.5$.

Concerning the curves $\beta(r)$, a similar approach may be taken. The cnoidal wave shape is obtained for $\phi = -\pi/2$, corresponding to the horizontal axis where $\beta = 0.5$ (acceleration under the crest equal to the acceleration under the trough). For the other values of ϕ, the figure shows that β is almost proportional to r, in the range $-\pi/2 < \phi < 0$.

For r *versus* α, Fig. 5 shows that α decreases (nonlinearly) with increasing values of r and the waveform parameter ϕ. Note that the particular case of $\phi = 0$ verifies the simple relation between α and r:

$$r = \cos(\pi \cdot \alpha) \tag{15}$$

Each curve in Fig. 5 can be accurately parameterized by rational functions of 3rd order polynomials, of the form:

$$R \approx \frac{a_1 + b_1 \cdot r + r^3}{c_1 - d_1 \cdot r + e_1 \cdot r^2 + r^3} \tag{16}$$

$$\beta \approx \frac{a_2 + b_2 \cdot r + r^3}{c_2 - d_2 \cdot r + e_2 \cdot r^2 + r^3} \tag{17}$$

$$\alpha \approx \frac{a_3 + b_3 \cdot r + r^3}{c_3 - d_3 \cdot r + e_3 \cdot r^2 + r^3} \tag{18}$$

where a_i, b_i, c_i, d_i and e_i are fitting coefficients for each ϕ ($i = 1$, 2, and 3). The best values of those constants are presented in Table 1 for Eqs. (16), (17) and (18), respectively. The root mean square absolute errors (e_{RMS}) of the parameterized curves are presented in the last row of each table. The low e_{RMS} values found clearly show that the adopted functions (16) to (18), with the fitting coefficients given in Table 1, represent quite well the exact curves of Eq. (7) for the studied domain. The above set of rational 3rd order polynomials provided much closer agreement to the desired relationships than that

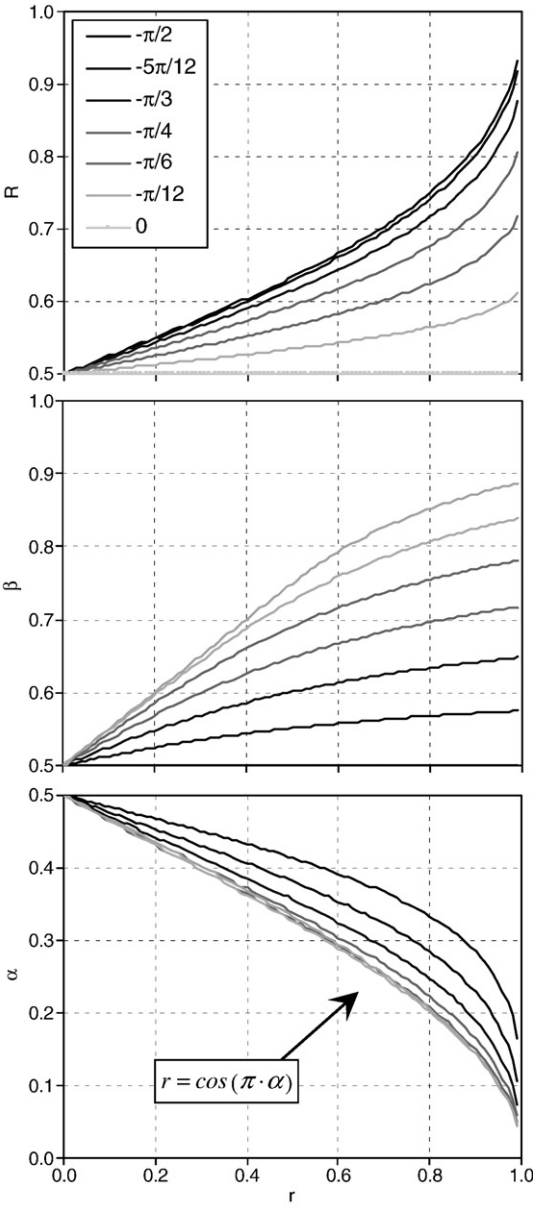

Fig. 5. *r versus R*, β and ϕ for $-\pi/2 \le \phi \le 0$.

obtained from other simpler functions (e.g., exponentials), that the observation of the curves in Fig. 5 may suggest.

For the practical use of the proposed wave form, Eq. (7), it is desirable to find a relation between the independent variables (r, ϕ) and (R, β), or (R, α), that is, inverting the pairs of Eqs. (16) and (17), or Eqs. (16) and (18). The advantage to use such parameterisations is that, given a set of desired values of R and β (or α), these expressions can be used to compute r and ϕ. For this purpose, we rewrite each of the Eqs. (16)–(18) as a cubic polynomial of r, whose roots are computed directly via Cardano's method (e.g., Anglin and Lambek, 1995). Combining the solutions of r resulting from the associations (R, β) or (R, α), it is possible to deduce the corresponding range of ϕ that simulates those asymmetries. Then, one can finally interpolate the values of r and ϕ to use directly as input in Eq. (7). In Appendix B, a step-by-step guide, explaining the previous methodology, is illustrated through a numerical example.

Also, the dependence between α and both velocity and acceleration parameters (R and β, respectively) has been obtained by changing ϕ (Fig. 6). As that asymmetry parameter is not required as an input in Eq. (7), no expression for β is given. All the same, Fig. 6 evidences the nonlinear relations between those parameters. For the "sawtooth" wave ($\phi = 0$), α changes, while R remains constant ($R = 0.5$, i.e., velocity under the crest equal to the velocity under the trough). For a constant ϕ, α decreases almost linearly with increasing values of R. Concerning α *versus* β (Fig. 6, lower panel), for $\phi = -\pi/2$ the corresponding line between the two parameters coincides with the vertical axis, where $\beta = 0.5$ (acceleration under the crest equal to the acceleration under the trough). For a fixed ϕ, the (α, β) relation shows a stronger nonlinearity than the (α, R) relation, with α inversely proportional to β.

4. Comparison with other formulations

In this section, three different theoretical wave formulations given in the literature are tested against Eq. (7). The results suggest that the new expression can accurately reproduce those wave shapes, which turn out to be particular cases of it for most conditions.

4.1. Isobe and Horikawa (1982)

Isobe and Horikawa (1982) developed a hybrid wave theory which combines fifth-order Stokes wave theory with third-order cnoidal wave theory to compute the wave orbital motion, and it can be used in a wide range of wave conditions. Hereafter, the method will be referred as IH82. This theory is able to yield skewed and asymmetric wave forms, and will thus be compared with the present formulation.

The expressions of IH82 can be used to generate representative waves in terms of R and α and, following Dibajnia et al. (2001), the method is as follows:

$$u(t) = R \cdot 2U_w \cdot \sin\left(\frac{\pi t}{\alpha T}\right), \quad -\Theta_2 T \le t \le (\alpha - \Theta_2)T \tag{19}$$

$$u(t) = (1-R) \cdot 2U_w \cdot \sin\left(\frac{\pi[t - T(1+\Theta_1)]}{T - \alpha T}\right), \quad (\alpha - \Theta_2)T < t \le (1-\Theta_2)T \tag{20}$$

with

$$\Theta_1 = \frac{1-\alpha}{\pi}\arcsin\sqrt{\frac{\mu_u^2\mu_T^2 - 1}{\mu_u^2(\mu_T^2 - 1)}} - \Theta_2 \tag{21}$$

$$\Theta_2 = \frac{\alpha}{\pi}\arcsin\sqrt{\frac{\mu_u^2\mu_T^2 - 1}{\mu_T^2 - 1}} \tag{22}$$

$$\mu_u = \frac{1-R}{R} \tag{23}$$

$$\mu_T = \frac{1-\alpha}{\alpha} \tag{24}$$

The analysis of the expressions revealed discontinuities in the acceleration time series for $R \neq 0.5$, which are related with the boundary values of t in Eqs. (19) and (20). Because β relies on the extreme values of the fluid acceleration and the discontinuities are reflected in its calculation, it is recommended to reproduce the same kind of wave with Eq. (7) through the "wave skewness parameter" α.

The upper panel of Fig. 7 shows the orbital velocities from the IH82 method, for $R = 0.65$ and $\alpha = 0.30$, and the curve computed through Eq. (7). The wave represented has both velocity and acceleration skewness, corresponding to a value of ϕ in Eq. (7) between 0 and $-\pi/2$. The values for ϕ and r in Eq. (7) were obtained through interpolation of the parameterisations presented in Section 3, leading

Table 1
Fitting coefficients for Eq. (16).

ϕ	$-\pi/12$	$-\pi/6$	$-\pi/4$	$-\pi/3$	$-5\pi/12$	$-\pi/2$
a_1	6.883	6.489	7.699	7.775	7.793	7.702
b_1	−6.964	−7.197	−8.528	−8.687	−8.726	−8.645
c_1	13.798	12.975	15.315	15.375	15.321	15.115
d_1	16.030	17.557	21.672	22.539	22.815	22.655
e_1	2.728	3.983	5.560	6.259	6.562	6.596
e_{RMS}	4.06E−05	4.87E−06	1.00E−04	4.66E−04	9.50E−04	1.19E−03

Fitting coefficients for Eq. (17).

ϕ	0	$-\pi/12$	$-\pi/6$	$-\pi/4$	$-\pi/3$	$-5\pi/12$
a_2	0.195	0.072	0.122	0.383	1.169	2.179
b_2	0.182	0.090	0.006	−0.019	0.007	−1.607
c_2	0.391	0.144	0.245	0.767	2.341	4.363
d_2	0.028	−0.014	0.230	0.623	1.242	4.432
e_2	0.188	0.227	0.426	0.755	1.255	1.795
e_{RMS}	1.10E−04	2.81E−05	1.64E−05	4.53E−06	1.83E−06	1.10E−05

Fitting coefficients for Eq. (18).

ϕ	0	$-\pi/12$	$-\pi/6$	$-\pi/4$	$-\pi/3$	$-5\pi/12$
a_3	3.499	3.782	4.227	4.675	5.126	5.158
b_3	−4.481	−4.760	−5.199	−5.640	−6.078	−6.103
c_3	6.999	7.572	8.464	9.365	10.279	10.348
d_3	4.172	4.314	4.930	6.072	7.773	9.403
e_3	0.188	0.227	0.426	0.755	1.255	1.795
e_{RMS}	3.00E−05	1.95E−05	2.30E−05	3.57E−05	5.47E−05	6.78E−05

to $\phi=-0.31\pi$ and $r=0.652$. Also, to have a comparable trend between the curves, a certain time lag, Δt, needs to be considered in the new formulation ($t'=t+\Delta t$), because for IH82 $t=0$ corresponds to a null velocity. This time lag corresponds to the zero up-crossing of the velocity time series of Eq. (7) and can be calculated as follows:

$$\Delta t = \frac{T \arcsin\left(\frac{-\sin\phi + \sqrt{-(1-r)(1+r)}\sin\phi}{r}\right)}{2\pi} \tag{25}$$

The lower panel of Fig. 7 contains the corresponding time series of the acceleration and clearly shows the two discontinuities associated with the time limits of Eqs. (19) and (20). Consequently, the new formulation seems more adequate as representative of both velocity and acceleration time series.

For the particular cases of sawtooth-shaped waves, some differences in the orbital velocity time series were found between the two formulations (Fig. 8). The corresponding indexes of skewness r used in Eq. (7) are presented in Fig. 8 and were computed according to Eq. (15). Although both formulations match at the instants of maximum and minimum values, the concavities of the curves differ between the wave crest and the wave trough for the lowest value of α (larger r). In that case,

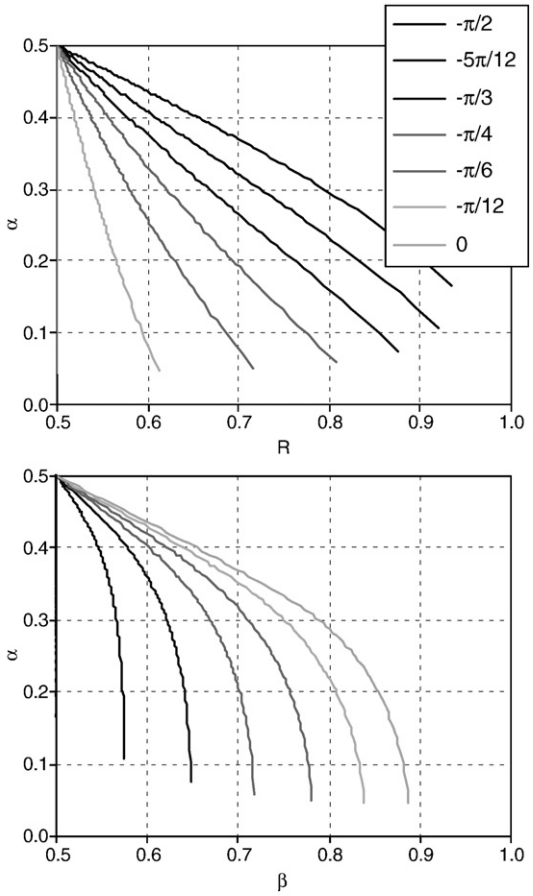

Fig. 6. α *versus* R and β for $-\pi/2\le\phi\le0$.

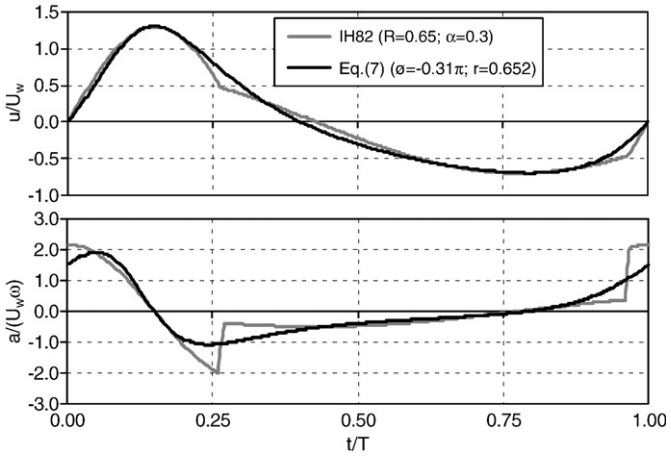

Fig. 7. Time varying orbital velocities and accelerations: comparison between IH82 formulation with $R=0.65$ and $\alpha=0.30$ *versus* Eq. (7) with $\phi=-0.31\pi$ and $r=0.652$.

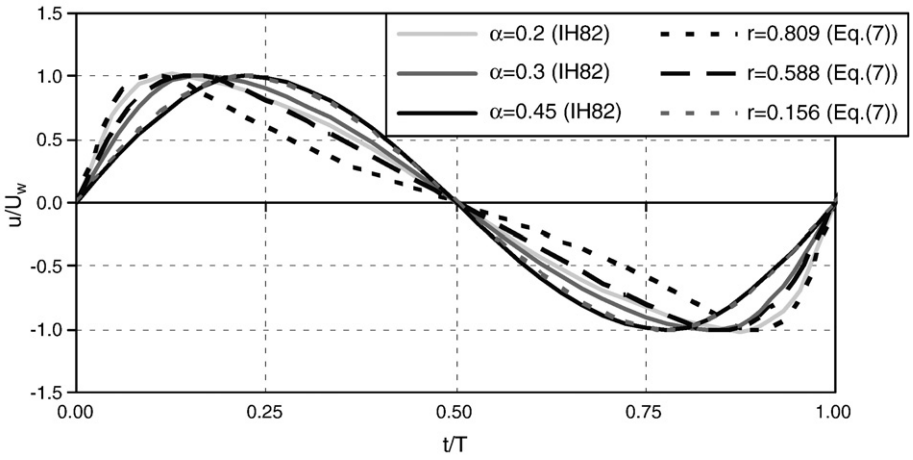

Fig. 8. Time varying orbital velocities: comparison between IH82 theory (—) and present formulation (---) for the sawtooth wave velocity profile ($\phi = 0$) and three values of the skewness index r.

the present solution provides a sharper (velocity) wave profile, with somewhat unrealistic curvatures immediately past the wave crest and prior to the wave trough. On the contrary, for larger values of α, the results are very consistent, e.g. for $\alpha = 0.45$, corresponding to a nearly sinusoidal wave, one can observe an almost perfect match between both curves. For the intermediate α value ($\alpha = 0.3$), the curves match considerably and it is difficult to assert which analytical curve is more representative of a real wave shape. The fact that the present approach does not fully represent the more theoretical formulation of Isobe and Horikawa (1982) is not a matter of concern, once the development of the new equation aims at providing a realistic nonlinear skewed wave shape, but not necessarily in perfect agreement with any other nonlinear theory.

4.2. Drake and Calantoni (2001)

In order to investigate the effect of the fluid acceleration on bedload transport in nearshore marine environments, Drake and Calantoni (2001) considered a near-bed orbital velocity representative of a wide range of shoaling and broken waves as described in Eq. (5). Hereafter, the method of Drake and Calantoni (2001) will be referred to as DC01.

The upper panel of Fig. 9 represents the dimensionless values of $u(t)$ (also shifted in time) obtained from DC01 and Eq. (7), for different values of the waveform parameter ($\phi = 0$, $-\pi/4$ and $-\pi/2$). The corresponding dimensionless values of $a(t)$ are shown in the lower panel of Fig. 9. The solutions for $u(t)$ with values of ϕ between the

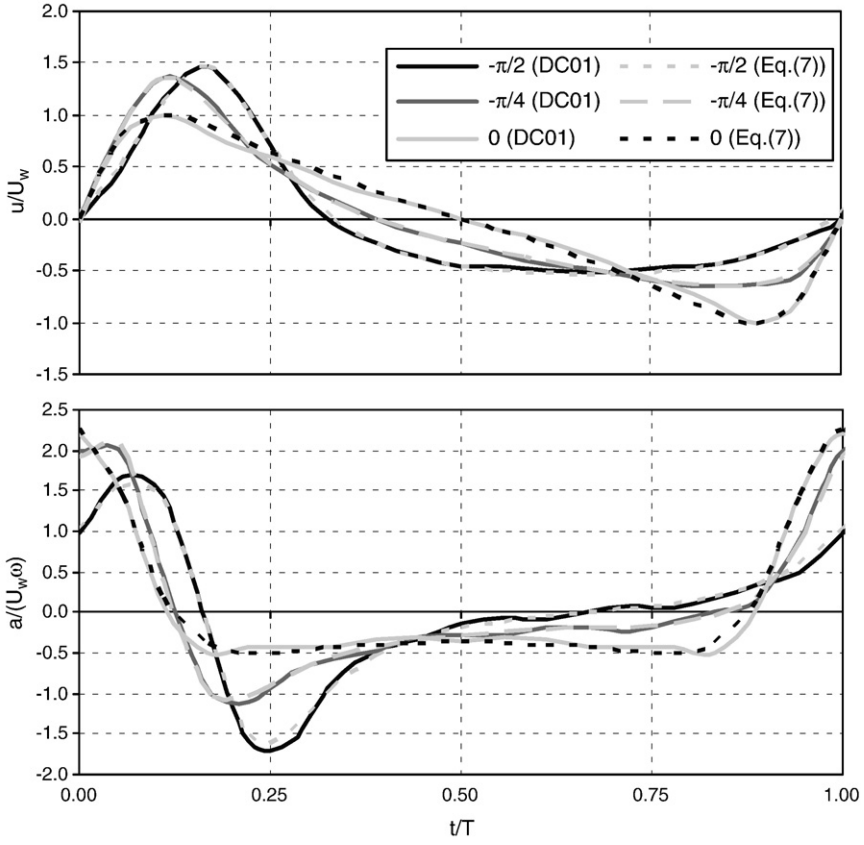

Fig. 9. Time varying orbital velocity and acceleration: comparison between DC01 theory (—) and Eq. (7) (---) for different ϕ values.

limits represented in the figure characterize a wide qualitative range of shoaling and broken waves. However, the values of the velocity and acceleration skewness parameters obtained for each ϕ following DC01 are fixed because the corresponding value of n in Eq.(7) is equal to 2. Table 2 presents these values for different values of ϕ. For the comparison Eqs. (16), (17) and the values of R and β corresponding to $\phi=0$, $-\pi/4$ and $-\pi/2$ in Table 2 were used to find the best approximation for the input parameter r in Eq. (7) ($r=0.766$, $r=0.805$ and $r=0.772$, respectively). It is further possible to distinguish that small fluctuations appear in the acceleration time series of DC01 solution, caused by the truncated five terms of the sum in Eq. (5). However, with the new formulation, those fluctuations disappear completely.

Fig. 10 further evidences that Drake and Calantoni's solution (dashed line) can be assumed as a particular solution of Eq. (7), given the unique relation of R and β corresponding to their solution, and contained by the field of solutions of the present formulae (shaded region).

4.3. Elfrink et al. (2006)

Recently, Elfrink et al. (2006) analysed a broad range of hydrodynamic conditions, corresponding to a large number of field data. In their work, a set of empirical formulations, describing important wave properties in shallow water, were derived using data mining techniques (evolutionary algorithms). Based on their proposed expressions, the continuous near-bed orbital velocity was expressed as:

$$\begin{aligned} u\left(t'\right) &= U_c \cdot \sin\left[1/2\pi t'/T_1\right], \quad 0<t'<T_1 \\ u\left(t'\right) &= U_c \cdot \cos\left[1/2\pi\left(t'-T_1\right)/(T_0-T_1)\right] \end{aligned} \tag{26}$$

$$-U_0 \sin\left[\pi(t-T_1)/(T_0-T_1)\right], \quad T_1<t'<T_0 \tag{27}$$

$$u\left(t'\right) = -U_t \cdot \sin\left[1/2\pi(t-T_0)/(T_2-T_0)\right], \quad T_0<t'<T_2 \tag{28}$$

$$u\left(t'\right) = -U_t \cdot \sin\left[1/2\pi(t-T_2)/(1-T_2)\right], \quad T_2<t'<1 \tag{29}$$

where t' is defined as $t'=t/T$. U_c, U_t, U_0 are velocity amplitudes and T_0, T_1 and T_2 are dimensionless instants associated to the time at maximum velocities and zero crossings. All these parameters are functions of the normalized wave height (H/h), normalized wave length (L/h) and the surf similarity parameter ξ. Hereafter, the method of Elfrink et al. (2006) is referred to as BE06.

The proposed expressions of BE06 for the time varying velocity result in discontinuous and non-smooth acceleration time series as already pointed out for the IH82 formulation. This is evidenced in Fig. 11 where BE06 solutions are compared against the new formulation (Eqs. (7) and (8)).These figures reproduce some of the cases given in Fig. 9 of Elfrink et al. (2006), for two waves with different lengths ($L/h=15$, 20) in a water depth of 2 m, $H/h=0.4$ and the bed slope equals 1:40. From Eq. (26)–(29) the corresponding values of R and α are, respectively, $R=0.66$ and $\alpha=0.28$ for $L/h=15$, and $R=0.63$ and $\alpha=0.22$ for $L/h=20$. Through the parameterisations presented in the previous section, one reached the values of $\phi=-0.29\pi$ and $r=0.699$ for $L/h=15$, and $\phi=-0.19\pi$ and $r=0.784$ for $L/h=20$.

Table 2
Values of R and β for different ϕ values in Drake and Calantoni (2001) formulation.

ϕ	0	$-\pi/12$	$-\pi/6$	$-\pi/4$	$-\pi/3$	$-5\pi/12$	$-\pi/2$
R	0.500	0.561	0.623	0.680	0.706	0.733	0.738
β	0.844	0.803	0.753	0.697	0.631	0.567	0.500

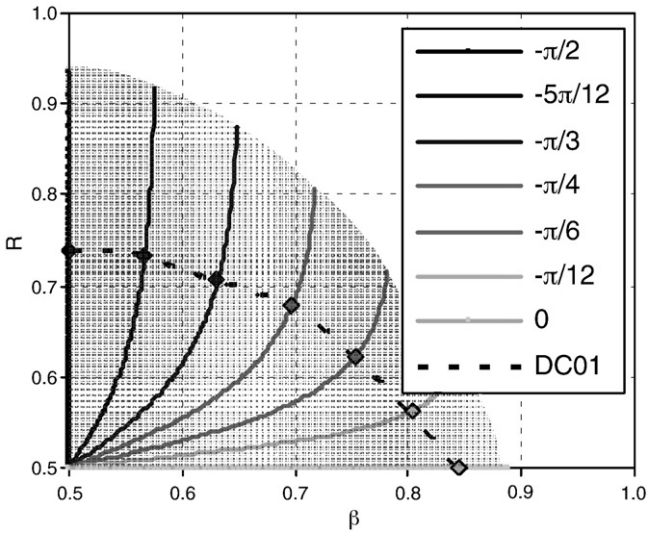

Fig. 10. Domain of solutions (β, R) for Eq. (7) (shaded area) and for DC01 (dashed line).

Fig. 11 shows a good match of both velocity time series, but differences are clear in the corresponding accelerations time series. The BE06 method presents discontinuities in the acceleration associated with the limits of Eqs. (26)–(29). The largest discrepancies are observed at the zero up-crossing of $u(t)$.

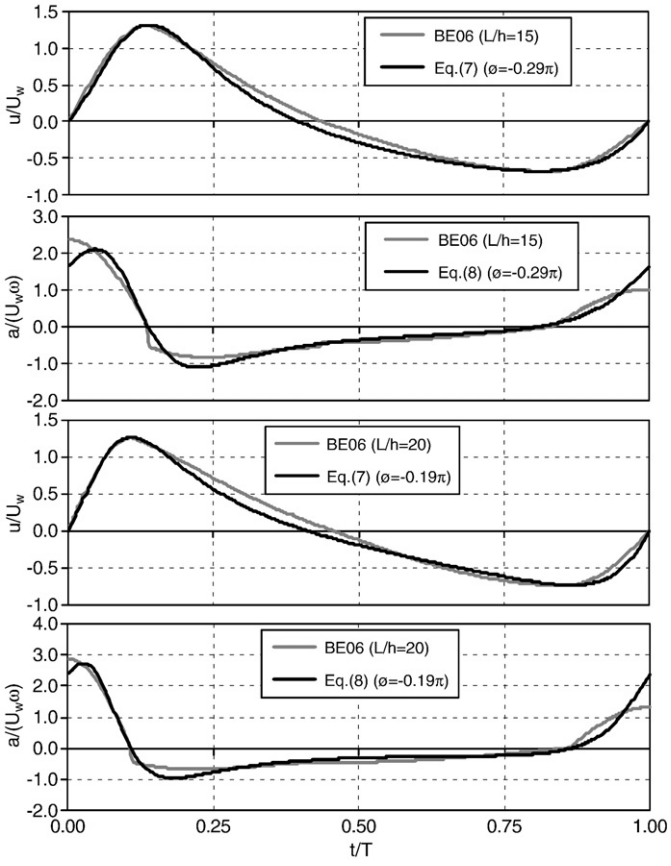

Fig. 11. Comparison of orbital velocity and acceleration time series computed from Eq. (7) and (8), and BE06 with $H/h=0.4$, $h=2$ m, slope 1:40, and varying L/h. The reproduction with Eq. (7) and (8) are accomplished with $\phi=-0.29\pi$ and $r=0.699$, and $\phi=-0.19\pi$ and $r=0.784$.

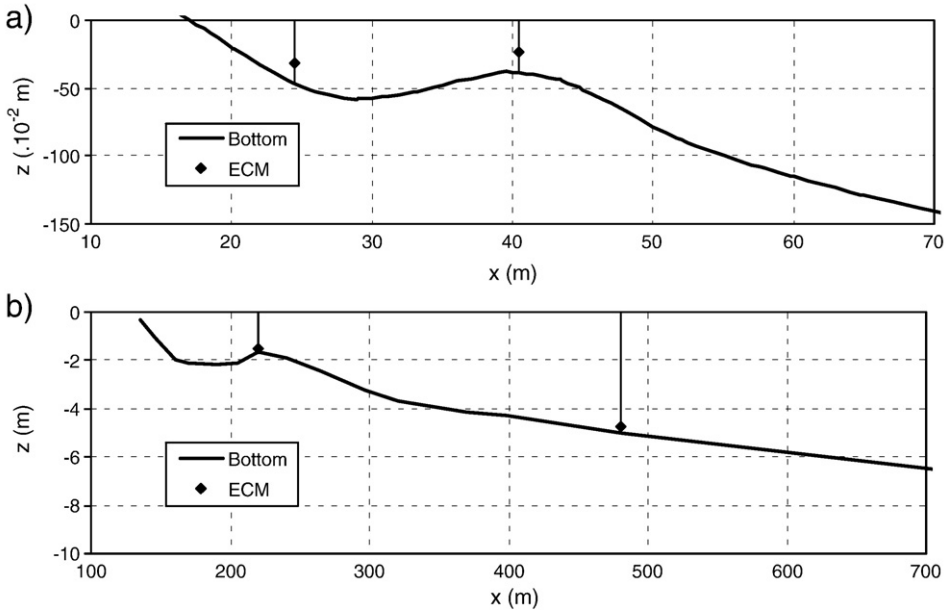

Fig. 12. Cross-shore bottom profiles (—) and positions of electromagnetic current meters (ECM) (♦) used in the data analysis: a) UPC experiment; b) DUCK94 experiment (October, 1st).

5. Simulation of measured velocity time series

In this section, we simulate measured near-bed velocity time series by means of Eq. (7). The analysis reflects a number of situations in shallow water with significant velocity and acceleration asymmetries. The simulated time series concern positions prior to, over and past a breaker-bar (Fig. 12) for two experimental conditions, one in a large-scale experiment (Sancho et al., 2001) and another in the field (DUCK94 campaign, Birkemeier and Thornton, 1994).

For the present purpose, the selected velocity records were transformed into a set of individual waves, delimited by two successive zero up-crossings. Each wave is associated with a value of U_w, ($U_w = (u_{max} - u_{min})/2$), and of the asymmetry coefficients R and α (Eqs. (1) and (4), respectively). The input parameters r and ϕ used in Eq. (7) were calculated for each wave considering the combinations (R, α) through the methodology described in Section 3 and Appendix B. We further remark that the use of the input parameters (R, α) is preferable to using the combination (R, β) because the latter implies differentiating the velocity records in order to compute β, whereas the former can easily be computed directly from the time series analysis of $u(t)$.

The first data set is reported in Sancho et al. (2001), and concerns the velocity records measured in the large-scale wave flume of the Polytechnic University of Catalonia (UPC), aimed at studying the

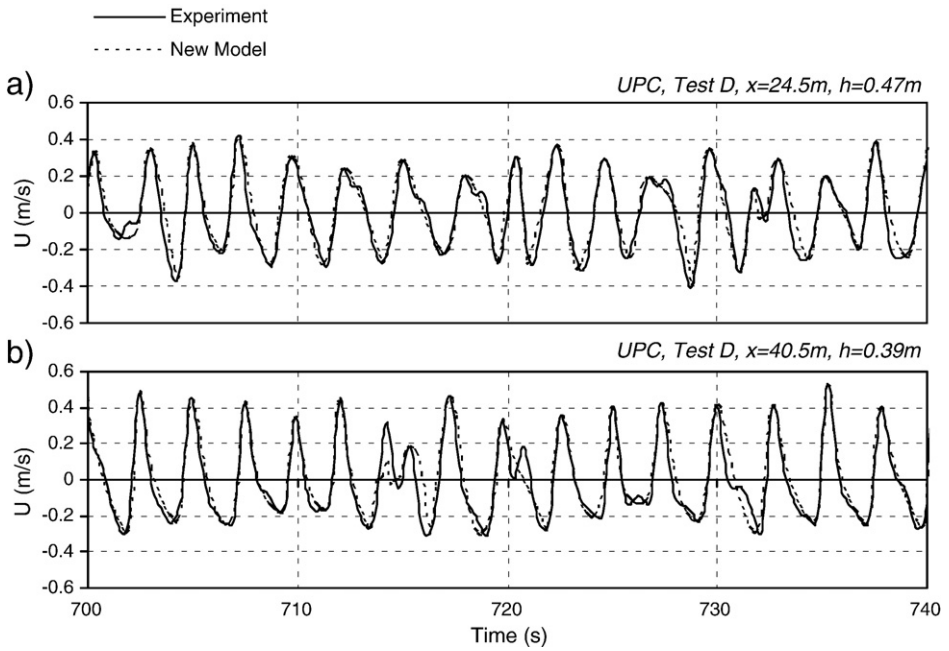

Fig. 13. Velocity time series: present model (---) and UPC experiment (—). (Refer to x-positions in Fig. 12a).

wave-induced turbulence and undertow over a fixed-bed, barred beach. Several instruments were deployed at several positions along the wave flume but, for the present analysis, we focus solely on the records provided by the electromagnetic current meters (ECM) in the 0.30 m layer above the bottom and at $x=24.5$ m and $x=40.5$ m. The data were gathered at 8 Hz sampling frequency. The experiments considered, amongst others, an irregular sea state described by a Jonswap spectrum, with a peak enhancement factor equal to 3.3, and $H_{rms}=0.21$ m and $T_p=2.5$ s in front of the wave maker (where $h=2.05$ m).

The second data set corresponds to the DUCK94 nearshore field experiment (Birkemeier and Thornton, 1994), performed by the Coastal and Hydraulics Laboratory of the U.S. Army Corps of Engineers at its Field Research Facility located in Duck, North Carolina (U.S.A.). This experiment provided high quality real data, aimed at understanding the complex phenomena associated with sand transport under waves and currents, and beach morphological evolution. In this study, we analyse the data of the SPUVT array (http://dksrv.usace.army.mil/jg/dk94dir) for the near-bottom (less than 30 cm) cross-shore velocities at two positions, $x=220.23$ m and $x=480.34$ m (lower panel of Fig. 12). The velocities were sampled at 2 Hz.

For the following analysis, the velocities from both data sets were high-pass filtered in order to remove low-frequency motions, since the present formulation aims at reproducing the waveform of single waves, with zero net current. Accounting for low-frequency oscillations in the velocity records would enhance deviations from that requirement, and hence such oscillations were filtered out. The high-pass frequency cut-off was set at approximately half of the peak frequency, namely, at 0.25 Hz for the UPC data and at 0.05 Hz for the DUCK experiment. For the UPC velocity data, higher-frequency oscillations (for $f>2$ Hz) were further removed in order to avoid spurious oscillations in the velocity time series, mainly associated with surf zone turbulence.

The comparison between the experimental UPC results and the simulated time series by means of Eq. (7) is given in Fig. 13. An overall quite satisfactory agreement is evident. Most wave forms are well reproduced, both over the bar-crest (panel b), where mostly broken waves propagate (Sancho, 2002), and past the bar-trough, where non-broken waves have reformed (panel a). Part of the discrepancies in some waves is due to the high-frequency fluctuations, with $f<2$ Hz, discernible in the measured velocities. Because the new formulation re-creates an equivalent wave with the same R and α values, such high-frequency fluctuations within the principal wave are not possible to be reproduced with the new expression.

Concerning the DUCK94 time series model-data comparison (Fig. 14), one perceives a non-negligible number of mismatches. These occur mainly for individual waves in which the velocity magnitude at the crest is smaller than at the trough, corresponding to conditions when $R<0.5$. Indeed, our parameterisations were validated in the region $R>0.5$, and thus, one could not expect a good agreement for the waves with such small values of R. Other mismatches occur in cases where the average measured velocity differs considerably from zero and our parameterisations consider a null averaged value. Nevertheless, there is a general good agreement between measurements and model predictions.

6. Conclusions

A new analytical approximate formulation for the wave form in the coastal zone is presented. The expression is very concise and requires the input of 4 parameters: amplitude of the orbital velocity, U_w; the angular frequency ω; an index of skewness r; and a waveform parameter ϕ. The new function can be used to describe the evolution of wave nonlinearities quite well and it fulfils the requirement of zero mean velocity. The equation is mathematically straightforward and, when compared with other existing formulations in the literature, it surpasses some of their limitations and extend their conditions of applicability. The new function has the advantage that it reproduces wave shapes for any combination of velocity and acceleration skewness parameters, generalizing the DC01 formulation and, moreover, it provides a continuous acceleration time series surpassing the mismatches of IH82 and BE06 formulations.

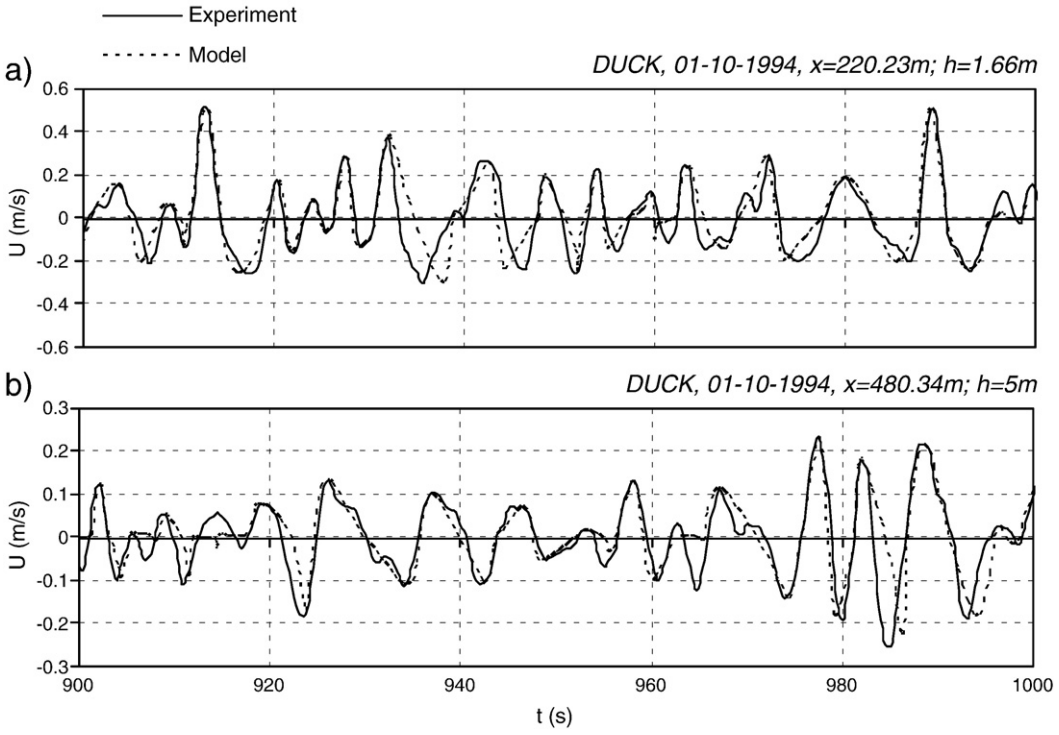

Fig. 14. Velocity time series: present model (---) and DUCK94 experiment (—). (Refer to x-positions in Fig. 12b).

For practical applications several parameterisations of macro-scale wave velocity and acceleration asymmetry indexes, (R, α and β), have been proposed. These are all similar polynomial functions (Eqs. (16)–(18)) of the input parameters r and ϕ, that provide an excellent fit to the mathematically unmanageable theoretical relations. For reproducing a wave with the velocity or the acceleration time series close to the shape of a 1st-order cnoidal wave, one should observe the restriction to the limit $r<0.6$.

The expression has been validated against field and laboratory experiments, revealing that the function can represent with reasonable accuracy the time varying near-bed orbital velocities, measured in the nearshore region, under breaking and non-breaking waves.

The equation is sufficiently general to be applied to a wide variety of nonlinear waves and it can be used for several practical engineering purposes; for example it can provide the wave forcing in experimental facilities (e.g., Silva et al., 2008) or in numerical modelling (e.g. Ruessink et al., 2009). Also, the inclusion of this formula in practical sediment transport formulae (e.g., Silva et al., 2006; Nielsen, 2006) enables the transport to be computed directly as a function of the velocity and acceleration skewness parameters.

As a final note, an expression has been proposed here for the near-bed horizontal orbital velocity, and the corresponding horizontal acceleration. It is envisaged that one may derive a corresponding equation for the free-surface displacement, based on an adequate description of the vertical variation of U_w and the wave celerity.

Acknowledgments

The first author has been supported by the Portuguese National Science Foundation (FCT) through a PhD grant (SFRH/BD/41827/2007). This work was also done within the research project "BRISA — BReaking waves Interaction with SAnd transport" (PTDC/ECM/67411/2006), supported by the FCT. The UPC data was collected within a project partly funded by the European Commission, Training and Mobility of Researchers Programme — Access to Large-scale Facilities (contract no. ERBFMGECT9500073), and the "Laboratorio de Ingenieria Maritima" (LIM) of the "Universitat Politècnica de Catalunya". The DUCK94 data was provided by the Field Research Facility, Field Data Collections and Analysis Branch, US Army Corps of Engineers, Duck, North Carolina. The new expression was studied and used in the TRANSKEW project on sediment transport under acceleration-skewed waves, supported by the European Community's Sixth Framework Programme through the Integrated Infrastructure Initiative HYDRALAB III, Contract no. 022441(RII3). The authors wish to thank Dr. Hervé Michallet for his invaluable comments and discussions held during a visit to Grenoble supported by the transnational agreement FCT/CNRS 2009 — Proc. 441.00.

We would also like to thank one of the anonymous reviewers for his comments that contribute to the clarity of some points in the text.

Appendix A

Eq. (6) in Section 2,

$$u(t) = U_w \sum_{k=0}^{\infty} \frac{1}{n^k} \sin\left[(k+1)\omega t + k\phi\right] \tag{I.1}$$

is equivalent to:

$$u(t) = U_w \mathrm{Im}\left[\sum_{k=0}^{\infty} \frac{1}{n^k} \exp(i[(k+1)\omega t + k\phi])\right] \tag{I.2}$$

Assuming

$$x = \left(\frac{1}{n}\right) \exp\left[i(\omega t + \phi)\right] \tag{I.3}$$

Eq. (I.2) can be written as:

$$u(t) = U_w \mathrm{Im}\left[\sum_{k=0}^{\infty} x^k \exp(i\omega t)\right] \tag{I.4}$$

The sum of such Taylor series can be exactly computed within the case of analytical functions with complex variables:

$$u(t) = U_w \mathrm{Im}\left[\left(\frac{1}{1-x}\right) \exp(i\omega t)\right] \tag{I.5}$$

with

$$\mathrm{Im}\left[\left(\frac{1}{1-x}\right) \exp(i\omega t)\right] = n\frac{(n\sin(\omega t) + \sin\phi)}{(1 + n^2 - 2n\cos(\omega t + \phi))} \tag{I.6}$$

Thus, Eq. (I.1) results in:

$$u(t) = U_w f \frac{\left[\sin(\omega t) + \frac{r\sin\phi}{1+\sqrt{1-r^2}}\right]}{[1 - r\cos(\omega t + \phi)]} \tag{I.7}$$

where $r = 2n/(1+n^2)$ and f is a dimensionless factor that subsumes the quotient $n^2/(1+n^2)$ in Eq. (I.7) and forces the velocity amplitude to be equal to U_w. f is only function of r, obeying the relation $f = \sqrt{1-r^2}$.

Appendix B

Appendix B.1. Interpolation procedure

In the following, a short guide is provided, illustrating the approach used to obtain the values (r, ϕ) from the knowledge of (R, α). The latter key parameters can be obtained from the knowledge of the wave height, wave period, local water depth and bottom slope (e.g., Dibajnia et al., 2001; Tajima and Madsen, 2002; Tajima, 2004; and Elfrink et al., 2006). For the explanation one uses the example given in Section 4.3, of a wave with normalized wave length and wave height, respectively, of $L/h = 15$ and $H/h = 0.4$, propagating at 2 m depth over a beach with slope equal to 1:40 (Elfrink et al., 2006). The corresponding values of R and α are $R = 0.659$ and $\alpha = 0.278$. To find the corresponding pair (r, ϕ) values the following methodology is proposed:

i) Using Eq. (16) with $R = 0.659$ it is possible to estimate r for each ϕ of Table 1 by inverting such equation (yielding a 3rd-order polynomial) and finding its roots via Cardano's method. This method returns three solutions of r, but only the real solution within $0<r<1$ is accepted. Applying Eq. 18 for those values of r, one finds a set of α values. It is then possible to limit the range of ϕ within our domain ($-\pi/2 \le \phi \le 0$), verifying in which ϕ values $\alpha = 0.278$ is included. For $\alpha = 0.278$, we are restricted to $\phi = -\pi/4$ ($r = 0.7449, \alpha = 0.248$) and to $\phi = -\pi/3$ ($r = 0.6480$ and $\alpha = 0.308$). We proceed then with linear interpolation and find $\phi = -0.286\pi$ for $\alpha = 0.278$.
ii) An analogous procedure can be used starting with α, i.e., using Eq. (18) with $\alpha = 0.278$ it is possible to estimate r, for each ϕ of Table 1, via Cardano's method. Applying Eq. (16) with these values of r one calculates a set of R values, and delimitates the range of ϕ within our domain ($-\pi/2 \le \phi \le 0$), verifying the ϕ values in which $R = 0.659$ is included. For $\alpha = 0.278$ we are restricted to $\phi = -\pi/4$ ($r = 0.6704$ and $R = 0.637$) and to $\phi = -\pi/3$ ($r = 0.7300$ and $R = 0.689$). From linear interpolation, for $\alpha = 0.278$ we obtain $\phi = -0.292\pi$.
iii) The average value of ϕ, computed in i) and ii), is considered the final ($\phi \approx -0.29\pi$).
iv) The value of ϕ in step iii) is used to compute the final r. Firstly, the final values in step i) ($r = 0.7449$ and $r = 0.6480$ corresponding,

respectively, to $\phi=-\pi/4$ and $\phi=-\pi/3$) are used to obtain a first solution ($r=0.700$). Secondly, the final values in step ii) ($r=0.6704$ and $r=0.7300$ corresponding, respectively, to $\phi=-\pi/4$ and $\phi=-\pi/3$) are used to obtain a second solution ($r=0.698$). Then, the average value is considered the final approach ($r\approx0.699$).

Following the above procedure, which is not exact, the errors for predicting ϕ and r are approximately 3.4% and 2.5%, respectively, within the range $-\pi/2\leq\phi\leq0$ and $0<r<1$.

References

Anglin, W.S., Lambek, J., 1995. Mathematics in the Renaissance. The Heritage of Thales, Ch. 24. Springers.

Bailard, J.A., 1981. An energetics total load sediment transport model for a plane sloping beach. J. Geophys. Res. 86 (C11), 10938–10954.

Birkemeier, W.A., Thornton, E.B., 1994. The DUCK94 nearshore field experiment. Proceedings of the Conference on Coastal Dynamics '94, ASCE, pp. 815–821.

Dibajnia, M., Moriya, T., Watanabe, A., 2001. A representative wave model for estimation of nearshore local transport rate. Coastal Engineering Journal 43 (1), 1–38.

Drake, T.G., Calantoni, J., 2001. Discrete particle model for sheet flow sediment transport in the nearshore. Journal of Geophysical Research — Oceans 106 (C9), 19859–19868.

Elfrink, B., Hanes, D.M., Ruessink, B.G., 2006. Parameterization and simulation of near bed orbital velocities under irregular waves in shallow water. Coastal Engineering 53, 915–927.

Elgar, S., Guza, R.T., 1985. Observations of bispectra of shoaling surface gravity waves. J. Fluid Mech. 161, 425–448.

Elgar, S., Gallagher, E.L., Guza, R.T., 2001. Nearshore sand bar migration. J. Geophys. Res. 106 (C6), 11623–11627.

Hoefel, F., Elgar, S., 2003. Wave-induced sediment transport and sandbar migration. Science 299, 1885–1887.

Hsu, T.-J., Hanes, D.M., 2004. The effect of wave shape on sheet flow sediment transport. J. Geophys. Res. 109, C05025.

Isobe, M., Horikawa, K., 1982. Study on water particle velocities of shoaling and breaking waves. Coast. Eng. Jpn 25, 109–123.

Leykin, I.A., Donelan, M.A., Mellen, R.H., McLaughlin, D.J., 1995. Asymmetry of wind waves studied in a laboratory tank. Nonlinear Processes in Geophysics, European Geophysical Society 2, 280–289.

Nielsen, P., 1992. Coastal Bottom Boundary Layers and Sediment Transport. World Sci, Singapore. 324 pp.

Nielsen, P., 2006. Sheet flow sediment transport under waves with acceleration skewness and boundary layer streaming. Coastal Engineering 53, 749–758.

Ribberink, J., Al-Salem, A., 1994. Sediment transport in oscillatory boundary layers in cases of rippled beds and sheet flow. J. Geophys. Res. 99 (C6), 12707–12727.

Ruessink, B.G., van den Berg, T.J.J., van Rijn, L.C., 2009. Modeling sediment transport beneath skewed-asymmetric waves above a plane bed. J. Geophys. Res. 114, C11021. doi:10.1029/2009JC005416.

Sancho, F., 2002. Surface wave statistics past a barred beach. Proceedings of 6th Congress of the Italian Society for Applied and Industrial Mathematics (SIMAI), Chia Laguna (Italy).

Sancho, F., Mendes, P.A., Carmo, J.A., Neves, M.G., Tomasicchio, G.R., Archetti, R., Damiani, L., Mossa, M., Rinaldi, A., Gironella, X., Arcilla, A.S., 2001. Wave hydrodynamics over a barred beach. Proceedings of the International Symposium on Ocean Wave Measurement and Analysis — "Waves 2001", S. Francisco, ASCE.

Silva, P.A., Temperville, A., Santos, F.S., 2006. Sand transport under combined current and wave conditions: a semi-unsteady, practical model. Coastal Engineering 53, 897–913. doi:10.1016/j.coastaleng.2006.06.010.

Silva, P.A., Abreu, T., Sancho, F., Temperville, A., 2007. A sensitivity study of sediment transport rates in accelerated skewed waves. In: Dohmen- Janssen, M., Hulscher, S. (Eds.), Proceedings of the 5th IAHR Symposium on River. : Coastal and Estuarine Morphodynamics. Enschede, The Netherlands, pp. 337–343.

Silva, P.A., Abreu, T., Freire, P., Kikkert, G., Michallet, H., O'Donoghue, T., Plecha, S., Ribberink, J., Ruessink, G., Sancho, F., Steenhauer, K., Temperville, A., Van der, V.A., Van der Werf, J., 2008. Sand transport induced by acceleration-skewed waves and currents — the TRANSKEW project. PECS08 — Physics of Estuaries and Coastal Seas, Liverpool, UK, pp. 163–166.

Soulsby, R.L., Damgaard, J.S., 2005. Bedload sediment transport in coastal waters. Coastal Engineering 52, 673–689.

Stokes, G.G., 1847. On the theory of oscillatory waves. Trans. Camb. Philos. Soc. 8, 441–455.

Suntoyo,, Tanaka, H., Sana, A., 2008. Characteristics of turbulent boundary layers over a rough bed under saw-tooth waves and its application to sediment transport. Coastal Engineering 55 (12), 1102–1112.

Svendsen, I.A., 2006. Introduction to nearshore hydrodynamics. In: Liu, P. (Ed.), Advanced Series on Ocean Engineering, 24. World Scientific. pp. 722.

Svendsen, I.A., Madsen, P.A., Buhr Hansen, J., 1978. Wave characteristics in the surf zone. Proceedings of the 16th International Conference on Coastal Engineering, Hamburg, ASCE, vol. 1, pp. 520–539.

Tajima, Y., 2004. Waves, currents, and sediment transport in the surf zone along long, straight beaches. PhD thesis, Massachusetts Institute of Technology, Cambridge, MA.

Tajima, Y., Madsen, O.S., 2002. Shoaling, breaking and broken wave characteristics. Proceedings of the 28th International Conference on Coastal Engineering. World Scientific, pp. 222–234.

Torres-Freyermuth, A., Losada, I.J., Lara, J.L., 2007. Modeling of surf zone processes on a natural beach using Reynolds-averaged Navier–Stokes equations. J. Geophys. Res. 112, C09014.

Van der A, D.A., O'Donoghue, T., Davies, A.G., Ribberink, J.S., 2008. Effects of acceleration skewness on rough bed oscillatory boundary layer flow. Proceedings of the 31st International Conference on Coastal Engineering, Hamburg, ASCE, pp. 1583–1595.

Watanabe, A., Sato, S., 2004. A sheet-flow transport rate formula for asymmetric, forward-leaning waves and currents. Proceedings of the 29th International Conference on Coastal Engineering, Lisbon, ASCE, vol. 2, pp. 1703–1714.